BNL-108285-2015-JA

THE JOURNAL OF PHYSICAL CHEMISTRY C

Subscriber access provided by BNL Research Library

Article

Structural Changes in Self-Catalyzed Adsorption of Carbon Monoxide on 1,4-Phenylene Diisocyanide-Modified Au(111)

John Kestell, J. Anibal Boscoboinik, Lanxia Cheng, Michael Garvey, Dennis W. Bennett, and Wilfred T. Tysoe

J. Phys. Chem. C, **Just Accepted Manuscript** • DOI: 10.1021/acs.jpcc.5b04783 • Publication Date (Web): 23 Jul 2015

Downloaded from http://pubs.acs.org on July 31, 2015

Just Accepted

"Just Accepted" manuscripts have been peer-reviewed and accepted for publication. They are posted online prior to technical editing, formatting for publication and author proofing. The American Chemical Society provides "Just Accepted" as a free service to the research community to expedite the dissemination of scientific material as soon as possible after acceptance. "Just Accepted" manuscripts appear in full in PDF format accompanied by an HTML abstract. "Just Accepted" manuscripts have been fully peer reviewed, but should not be considered the official version of record. They are accessible to all readers and citable by the Digital Object Identifier (DOI®). "Just Accepted" is an optional service offered to authors. Therefore, the "Just Accepted" Web site may not include all articles that will be published in the journal. After a manuscript is technically edited and formatted, it will be removed from the "Just Accepted" Web site and published as an ASAP article. Note that technical editing may introduce minor changes to the manuscript text and/or graphics which could affect content, and all legal disclaimers and ethical guidelines that apply to the journal pertain. ACS cannot be held responsible for errors or consequences arising from the use of information contained in these "Just Accepted" manuscripts.

ACS Publications

The Journal of Physical Chemistry C is published by the American Chemical Society. 1155 Sixteenth Street N.W., Washington, DC 20036
Published by American Chemical Society. Copyright © American Chemical Society. However, no copyright claim is made to original U.S. Government works, or works produced by employees of any Commonwealth realm Crown government in the course of their duties.

Structural Changes in Self-Catalyzed Adsorption of Carbon Monoxide on 1,4-Phenylene Diisocyanide-Modified Au(111)

John Kestell,[1] J. Anibal Boscoboinik,[2] Lanxia Cheng,[1] Michael Garvey,[1] Dennis W. Bennett[1] and Wilfred T. Tysoe[1] *

[1] *Department of Chemistry and Laboratory for Surface Studies, University of Wisconsin-Milwaukee, Milwaukee, WI 53211, USA*

[2] *Brookhaven National Laboratory, Center for Functional Nanomaterials, Upton, NY 11973, USA*

Abstract

The self-accelerated adsorption of CO on 1,4-phenylene diisocyanide- (PDI) derived oligomers on Au(111) is explored by reflection-absorption infrared spectroscopy and scanning tunneling microscopy. PDI incorporates gold adatoms from the Au(111) surface to form one-dimensional –(Au–PDI)$_n$– chains that can also connect between gold nanoparticles on mica to form a conductive pathway between them. CO adsorption occurs in two stages; it first adsorbs adjacent to the oligomers that move to optimize CO adsorption. Further CO exposure induces PDI decoordination to form Au–PDI adatom complexes thereby causing the conductivity of a PDI-linked gold nanoparticle array on mica to decrease to act as a chemically drive molecular switch. This simple system enables the adsorption process to be explored in detail. DFT calculations reveal that both the –(Au–PDI)$_n$– oligomer chain and the Au–PDI adatom complex are stabilized by co-adsorbed CO. A kinetic "foot-in-the-door" model is proposed in which fluctuations in PDI coordination allow CO to diffuse into the gap between gold adatoms to prevent the PDI from reattaching, thereby allowing additional CO to adsorb, to provide kinetic model for allosteric CO adsorption on PDI-covered gold.

Keywords: 1,4-phenylene diisocyanide (PDI), Au(111), carbon monoxide, molecular switch, allosteric effects.

* Author to whom correspondence should be addressed. E-mail: wtt@uwm.edu

Introduction

Adsorbate-induced structural changes are central to understanding allosteric effects in proteins and enzymes, [1] the classical example being the uptake of oxygen by hemoglobin.[2] Analogous adsorbate-induced structural changes have been found for carbon monoxide absorption in three-dimensional metal-organic frameworks (MOFs) that expose additional adsorption sites for the uptake of relatively weakly bound CO [3] resulting in self-accelerating adsorption. The one-dimensional –(Au–PDI)$_n$– chains formed by PDI on Au(111) [4-16] have also been used as a model system to explore such effects; this one-dimensional structure adsorbs carbon dioxide in a self-catalyzed process in which the chains adapt their positions to accommodate the carbon dioxide.[17] This procees is facilitated by the mobility of the oligomers [18] due to the low chain-diffusion barrier.[19] Here we report on the structural changes to the –(Au–PDI)$_n$– chains as a result of carbon monoxide adsorption that involve both the lateral motion of the oligomers found for carbon dioxide, as well as a more profound structural change that involves reversible isocyanide decoordination to create additional carbon monoxide adsorption sites. The structural simplicity of this model system allows the mechanism and energetics of self-accelerated adsorption to be explored in detail. In particular, it is found that carbon monoxide stabilizes both the inital, –(Au–PDI)$_n$– chains and the final, decoordinated system so that the structural change is not thermodynamically driven. A kinetic "foot-in-the-door" model is proposed in which fluctuations in isocyanide binding allow carbon monoxide to rapidly diffuse on the surface to inhibit reformation of the oligomer chain.

The self-assembled –(Au–PDI)$_n$– oligomers linked between gold nanoelectrodes provide a conductive pathways between them.[18] Analogous cross-linked isocyanide complexes [20] have also been shown to be electrically conductive.[21-23] It is found that disruption of the oligomer chains by CO decreases the conductivity, thereby producing a chemically driven

ACS Paragon Plus Environment

molecular switch. The variation in conductivity with carbon monoxide pressure shows two distinct regimes, analogous to the adsorption behavior found for three-dimensional MOF structures.[3]

The oligomer structure has been confirmed by comparing the results of density functional theory (DFT) calculations with the measured infrared spectra and scanning tunneling microscopy (STM) images collected as a function of tip bias.[24] It is found that the aryl ring of the PDI lies parallel to the surface, but that the molecule is strained such that the isocyanide group is bent by ~12° away from the planar, gas-phase structure. Chain propagation occurs through a mobile, vertical Au–PDI adatom complex that inserts into the terminus of an isocyanide group of PDI bound to a step edge or a surface defect.[19]

Experimental Section

Infrared Spectroscopy

A Au(111) single crystal (Princeton Scientific) was cleaned using cycles of ion bombardment with 1 keV argon ions for 30 minutes (1 μA/cm^2), annealing to 900 K for 5 minutes and then to 600 K for 30 minutes. The sample could be cooled to 80 K by thermal contact to a liquid-nitrogen-filled reservoir and resistively heated to ~1200 K. Reflection-absorption infrared spectroscopy (RAIRS) data were collected with a Bruker Vertex spectrometer, typically for 1000 scans at a resolution of 4 cm^{-1} as described elsewhere.[25] 1,4-phenylene diisocyanide (PDI) was obtained commercially (Aldrich Chemicals, 99% purity) and was degassed at room temperature for 1 hour prior to each experiment and dosed via a home-built source as described previously.[4] CO was dosed via an uncalibrated directional dosing tube so that exposures are given in Torr s.

Scanning Tunneling Microscopy

STM measurements were made in a UHV chamber operating at base pressures of ~2×10^{-10} Torr after bakeout. STM experiments were performed using a RHK UHV 350 dual AFM/STM as described elsewhere,[4] along with the methods used to prepare the tungsten tip. PDI was dosed in the same way as for the infrared measurements, but CO was dosed by backfilling the chamber and exposures are quoted in Langmuirs, L (1L = 1×10^{-6} Torr s). Images were processed by background subtraction.

Gold Film Preparation and Conductivity Measurements

Gold nanoparticles were prepared by evaporating gold onto a cleaved mica (highest grade, Ted Pella) substrate in a vacuum chamber that was pumped by means of an ion pump operating at a base pressure of ~1×10^{-8} Torr, to yield gold nanoparticles that are ~ 8 nm in diameter.[18] The film thickness was monitored by means of a quartz crystal microbalance. Gold electrode pads ~200 nm thick were evaporated at the edge of the sample. The temperature was measured by means of a chromel-alumel thermocouple attached to the sample and the current versus voltage (I/V) characteristics were measured by applying a voltage using a D/A converter and the resulting current measured by means of a Keithly picoammeter monitored by means of an A/D converter to yield the I/V curve directly.

The gold-covered mica samples were exposed to PDI from a directional dosing tube that was incident on the sample which was held at 290 K. I/V curves were measured following each PDI exposure until a constant final resistance was obtained The effect of CO on the conductivity of a PDI-covered gold nanoparticle array was measured by pressurizing the chamber with CO (Airgas, 99.999% purity).

Theoretical Methods

DFT calculations were performed with the projector augmented wave (PAW) method [26-27] as implemented in the Vienna *ab initio* simulation package, VASP.[28-30] The exchange-

correlation potential was described using the generalized gradient approximation (GGA) of Perdew, Burke and Ernzerhof.[31] A cutoff of 400 eV was used for the planewave basis set, and the wavefunctions and electron densities were converged to within 1×10^{-5} eV. The first Brillouin zone was sampled with either a 4×4×1 (Figures S1 and S2) or a 2×4×1 (Figure 5) Γ-centered k-point mesh. Geometric relaxations were considered to be converged when the force was less than 0.02 eV/Å on all unrestricted atoms. Calculations were also performed by including van der Waals corrections using the method of Tkatchenko and Scheffler (TS).[32]

Results

In order to gauge the effects of CO adsorption on a PDI-saturated Au(111) surface, infrared spectra were collected as a function of CO exposure at 100 K and the results are displayed in Figure 1.[33] The bottom spectrum in Figure 1A was collected following exposure to PDI for 10 seconds with the sample held at ~300 K. The spectrum displays a N≡C stretching mode at ~2158 cm^{-1} and an out-of-plane C-H wagging mode at ~820 cm^{-1}, as found previously for PDI on Au(111).[24] Subsequent spectra show the effect of exposing the surface to CO, where a number of changes are evident. In the N≡C stretching region, the single feature at ~2158 cm^{-1} splits into two peaks with a sharp feature at ~2128 cm^{-1} and a broad peak centered at ~2172 cm^{-1}. In addition, the out-of-plane C-H mode at ~820 cm^{-1} shifts to a higher frequency (~843 cm^{-1}) and broadens. New modes appear at 2028 and 2002 cm^{-1} with increasing CO exposure where the 2028 cm^{-1} peak appears at lower exposures (~0.72×10^{-4} Torr s) than the ~2002 cm^{-1} feature (which starts to appear at ~1.04×10^{-4} Torr s), and continues to grow with increasing CO exposure, saturating in intensity at an exposure of ~1.68×10^{-4} Torr s, while the ~2028 cm^{-1} feature broadens and may include several CO adsorption states.

The effect of heating the sample is shown in the top spectra of Figure 1A. The infrared features appearing after CO exposure persist when heating to ~151 K while the ~2028 cm^{-1} feature disappears at slightly lower temperatures (from ~151 to 166 K) than the ~2002 cm^{-1} mode (~166 to 310 K). The original spectrum for PDI on Au(111) is restored on heating to ~310 K indicating that the Au–PDI chains are reformed, but a slight shift is found in the isocyanide stretching mode to 2164 cm^{-1}, likely due to the formation of shorter chains.[24]

Carbon monoxide adsorbed on stepped gold surfaces or evaporated films [34-39] has CO stretching frequencies between ~2100 and ~2125 cm^{-1}, thereby raising the possibility that the additional 2128 cm^{-1} feature is due to CO adsorbed on gold. In order to investigate this, and to aid in assigning the vibrational modes, a similar experiment was carried out using ^{13}CO and the results are displayed in Figure 1B, where the spectrum for ^{12}CO is shown for comparison. The shifts that would be expected based on the change in reduced mass on isotopic substitution are also indicated. First, the 2128 cm^{-1} mode should shift to 2081 cm^{-1} on substituting ^{13}C for ^{12}C; no peaks are detected at this frequency indicting that this mode is not due to CO. The mode at 2002 cm^{-1} shifts to 1955 cm^{-1}, close to the value of 1958 cm^{-1} predicted for ^{13}CO, confirming that the feature is due to molecular carbon monoxide. The feature at 2028 cm^{-1} shifts to 2005 cm^{-1} on substituting ^{13}CO for ^{12}CO, indicating that the normal mode that gives rise to this vibration also contains carbon from the carbon monoxide.

Comparison of the vibrational frequencies after CO adsorption with the infrared spectra of self-assembled monolayers (SAMs) of PDI on gold films and particles dosed from solution [5, 40-41] and on Au(111) [24] indicate that CO exposure has caused one end of the PDI in the oligomer chain to become de-coordinated to form a perpendicular Au–PDI adatom complex. Note that this change is induced by the CO with a vibrational frequency of 2028 cm^{-1} resulting in additional CO adsorbing on the surface with a vibrational frequency of ~2002 cm^{-1}.

STM images were also collected to explore the structural changes induced by CO co-adsorption and are displayed in Figure 2. The top image in Figure 2 shows a PDI-saturated Au(111) surface that had been heated to ~370 K to remove any possible second-layer PDI species. As found previously,[4, 24, 42] PDI forms close-packed, one-dimensional chains on the surface, where the chains are found to emanate from step edges. The effects of low CO exposures are shown in the bottom images in Figure 2. In the image in Figure 2A, collected following exposure to 0.6 L of CO at 120 K, the one-dimensional chains essentially remain intact, while additional small features can be discerned adjacent to the chains. This is more clearly evident in the expanded image in Figure 2B, which shows small protrusions adjacent to the Au–PDI chains, highlighted in red, that are ascribed to co-adsorbed CO. The average spacing between adjacent CO molecules is ~0.5 nm, and the molecules tend to adsorb preferentially adjacent to one side of the chain, although the diffuse CO images suggest that CO is somewhat mobile. This is confirmed by regions in which the interchain gap is larger, indicated by the red oval, suggesting that CO can diffuse along the $< 1\bar{1}0 >$ directions.

The effect of higher CO exposures is shown in Figure 3. A typical STM image of a surface exposed to 3.6 L of CO at ~120 K is shown in Figure 3A, with a magnified region shown in Figure 3B. Bright and dark regions are clearly evident with a periodicity along the chains of 1.02 ± 0.02 nm (Figure 3C), and between adjacent chains of ~1.45 nm (Figure 3D). Now there are clearly regions where the chains become disrupted. In addition, there are slightly brighter regions around the brightest spots, also evident as small protrusions between the highest peaks in the profile in Figure 3D. The heights difference between peaks in Figure 3C and 3D suggests that the valley between the brightest spots is ~0.8 Å above the surface, and the proposed locations of co-adsorbed CO, spaced by 5Å, are indicated as red dots on the figure.

It has been shown that the $–(Au–PDI)_n–$ oligomer chains can link between gold nanoparticles on a mica substrate to significantly lower the resistance due to conduction

through the chains that act as molecular wires.[18] This suggests that, if the PDI oligomers in the linking molecular wires between gold nanoparticles are disrupted by CO adsorption, the conductivity of such a film should be affected by dosing with CO. Accordingly a mica sample that was covered by gold nanoparticles and saturated with PDI to form oligomeric linkages between them was pressurized with CO in the same vacuum chamber in which they were synthesized. The results of this experiment are shown in Figure 4 which plots the percentage change in resistivity of the film as a function of CO pressure. At low pressures (up to ~5 Torr, Figure 4A) the resistance increases almost linearly with CO pressure (■) and is completely reversible (□). However, at higher pressures, the resistivity varies in two stages. Slow changes are found for CO pressures below ~400 Torr with a Langmurian type behavior [43] that saturates to yield a ~4% percent resistance change. A second stage is seen at higher pressures (Figure 4B) in which the resistance change accelerates rapidly up to one atmosphere (the maximum pressure tested), where the change is ~15%. The inset to Figure 4B confirms that no conductivity change occurs in the absence of PDI.

Discussion

Adsorbate Structures at Low CO Coverages

The influence of CO co-adsorption on PDI-saturated Au(111) occurs in two distinct stages. In the first stage, CO exhibits a vibrational frequency of ~2028 cm^{-1} (Figure 1), which shifts on isotopic substitution to ~2005 cm^{-1}. The initial CO adsorption is accompanied by a modest resistivity increase when a PDI-linked gold nanoparticle array on mica is pressurized with CO at ~300 K (Figure 4). Here, the additional carbon monoxide binds on the gold surface adjacent to the $–(Au–PDI)_n–$ oligomer chains on Au(111) (Figure 2). DFT calculations that included van der Waals interactions were used to explore how CO binds adjacent to the chain and the most stable structures are depicted in Figure S1. In all cases, PDI was stabilized by

between ~40 and 55 kJ/mol by CO co-adsorption with a CO adsorption energy of ~50 kJ/mol (see Table 1), much greater than that found for CO on clean Au(111).[44] Horizontal red lines are included in the depiction of the structures to indicate the initial positions of the PDI oligomer chains, revealing that, in some cases, binding causes the chain to translate to optimize CO binding, analogous to the behavior when co-adsorbing CO_2.[17] In particular, CO initially in site A1 caused the chain to translate to an adjacent site to form a structure identical to adsorption in site A2. In other cases, for example, for adsorption in sites A3, B2, B3 and H2, CO moves from its original position (indicated by green dots) so that the final adsorption sites of initial geometries H2 and B3 are identical. This preferential adsorption of CO on one side of the oligomer chains is in accord with the STM images (Figure 2B).

The temperature-dependent infrared data shown in Figure 1 were obtained by heating the sample at ~1 K/s to the indicated temperature and then cooling back to ~120 K before collecting each spectrum. The temperature-dependent variation in coverage, estimated from the integrated areas of the infrared features, can therefore be used to estimate the CO desorption energy.[45] This analysis is carried out for the intensity changes of the low-coverage feature at 2028 cm^{-1} using a pre-exponential factor of 1×10^{16} s^{-1} [46] with a heating rate of 1 K/s to yield a value of desorption activation energy of 55 ± 5 kJ/mol,[45] in agreement with the calculated binding energy (Table 1).

Adsorbate Structures at High CO Coverages

Further CO dosing gives rise to an additional infrared feature due to CO at ~2002 cm^{-1}, as well as features at 2172 and 2128 cm^{-1} assigned to the formation of a vertical Au–PDI adatom complex. Perpendicular PDI molecules now image as bright spots with a spacing between them that is close to the periodicity of the initial Au–PDI oligomer chain (Figure 3) indicating that each gold adatom is coordinated to a single, vertical PDI molecule to form an Au–PDI adatom complex surrounded by co-adsorbed CO molecules. Some chain disruption occurs in less close-packed regions of the surface, for example at the top left of the image in Figure 3,

consistent with the mobility of the Au–PDI adatom complex.[19] However, the adatom complexes in the closer-packed regions of the surface remain relatively immobile due to crowding by co-adsorbed CO molecules that are now detected both adjacent to the rows and between the gold adatom complexes.

DFT calculations (including van der Waals interactions) were carried out to explore the stability of the vertical Au–PDI adatom complex and the influence of co-adsorbed CO. The most stable structures are displayed in Figure S2 and the calculated binding energies are summarized in Table 2. The heat of adsorption of an η^1 adatom complex, calculated from the energy difference between the structure shown in Figure S2A and the sum of the energies of gas-phase PDI and a Au(111) surface with a gold adatom is 152 kJ/mol. This is larger than the values of ~137 kJ/mol,[19] and 125 kJ/mol [8] obtained previously for the adatom complex calculated without van der Waals interactions. CO coadsorption stabilizes PDI bonding by ~44 kJ/mol, and CO binds with an energy of ~55 kJ/mol (Table 2). The CO binding energy for the state exhibiting the ~2002 cm^{-1} mode (Figure 1) is again estimated from the variation in intensity as a function of annealing temperature and again yields an energy that is in agreement with the calculated binding energy (Table 2).

Previous TPD experiments of a monolayer of PDI adsorbed on Au(111) at 300 K display a broad PDI desorption profile between ~325 and 500 K implying coverage-dependent desorption energies.[11] The desorption peak has a maximum temperature of ~400 K with a shoulder at ~475 K. A Redhead analysis yields activation energies from these states of ~105 and 125 kJ/mol respectively when using a pre-exponential factor of 1×10^{13} s^{-1}.[45]

The most plausible PDI desorption pathway from the $–(Au–PDI)_n–$ oligomer is via a two-step process in which PDI molecules in the chain initially decoordinate to form the adatom complex (Figure S2) before desorbing. As noted above, the energy of the rate-limiting step for this process lies between 105 and 125 kJ/mol. This energy range is in reasonable agreement with the calculated binding energies of the Au–PDI adatom complex (125 to 152

ACS Paragon Plus Environment

kJ/mol depending on whether van der Waals interactions are included). This implies that PDI desorption from the Au–PDI adatom complex is the rate-limiting step and therefore indicates that the energy to convert from the –(Au–PDI)$_n$– oligomer to the Au–PDI adatom complex is less than 125 to 105 kJ/mol.

Thus, CO adsorption stabilizes both the Au–PDI adatom complex and the –(Au–PDI)$_n$– oligomers by approximately the same amount. CO binding is also stabilized, consistent with the frequency shift from 2060 cm^{-1} for CO on clean Au(111).[39] The binding of isocyanides to gold is significantly stronger than CO while the electronic structures of CO and –N≡C are similar. In particular, while HNC is isoelectronic with CO, exhibiting the same ordering of 4σ, 1π, 5σ and 2π* orbitals, the orbital binding energies of the two molecules are very different such that the 5σ orbital of HNC lies within the gold d-bands [47] and is stabilized by ~5 eV when bound to gold. The corresponding antibonding orbital then shifts above the Fermi energy [48] thereby resulting in the formation of a strong σ-donor bond. A similar bonding structure has been found for vertical Au–PDI adatom complexes on Au(111).[49] In contrast, the CO 4σ, 1π and 5σ orbitals lie well below the bottom of the gold d-band, with the 2π* orbitals located close to the Fermi level [44] corresponding more closely to the conventional Blyholder model for CO adsorption on transition-metal surfaces.[50] However, the low density of states of gold near the Fermi level leads to only relatively weak back donation into the 2π* level, with CO acting as a weak π-acceptor, resulting in low binding energies. The PDI and CO stabilization are consistent with PDI acting as a σ-donor and CO as a π-acceptor.

Thermodynamics of PDI Decoordination

The above results indicate that co-adsorbed CO stabilizes <u>both</u> the –(Au–PDI)$_n$– oligomer chains <u>and</u> the Au–PDI adatom complex so that PDI decoordination is not thermodynamically facilitated by co-adsorbed CO. As discussed above, the energy to form the Au–PDI adatom complex from the –(Au–PDI)$_n$– oligomer chain is <105 to 125 kJ/mol. However, additional CO can adsorb on the surface, and STM images show that at least four CO molecules can

adsorb adjacent to the Au–PDI adatom complex (Figure 3), while two CO molecules can adsorb adjacent to the –(Au–PDI)– oligomer chains (Figure 2). An additional ~110 kJ/mol is gained by the adsorpion of the additional CO so that, if the energy to convert from the –(Au–PDI)$_n$– oligomer to the adatom complex is less than this value, the overall process becomes thermodynamically feasible.

Kinetics of PDI Decoordination

The energy barrier to convert between the oligomer chain and an Au–PDI adatom complex appears to be too high for this process to occur spontaneously at the CO dosing temperature of ~120 K. For example, even using a relatively low decoordination energy of ~40 kJ/mol calculated by neglecting van der Waals interactions (assuming a –(Au–PDI)$_n$– binding energy of 177 kJ/mol and an Au–PDI energy of 137 kJ/mol) results in a decoordination half-life of ~2500 s at 120 K assuming a pre-exponential factor of ~10^{13} s^{-1}.

Nudged elastic band (NEB) calculations for the growth of –(Au–PDI)$_n$– oligomer chains by the attachment of an mobile adatom complex to the terminus of a PDI molecule at a step suggest that the energy to decoordinate and slightly tilt the PDI molecule is ~29 kJ/mol,[19] and results in much shorter a half life of ~0.04 s for this process. Since PDI is constrained to remain in the vicinity of the adatom from which it decoordinates, it will ordinarily rapidly bind once again to the adatom, *unless something prevents it from doing so.* Carbon monoxide is suggested to kinetically inhibit the reverse reaction from occurring. It is proposed here that there is a high probability that CO molecules located adjacent to the decoordinated isocyanide will quickly move onto coordination sites between the gold adatoms, sterically impeding the PDI from reattaching.

In order to explore the feasibility of such a "foot-in-the-door" model, the most stable structure for a disrupted –(Au–PDI)$_n$– oligomer chain with a CO molecule bound to the gold adatom was calculated and the resulting most stable structures are shown in Figure 5. Figure 5A and 5B show top and side views of the initial –(Au–PDI)$_n$– oligomer chain calculated

ACS Paragon Plus Environment

using a larger 8×4 unit cell to include two PDI–Au units. The structure formed by placing a CO molecule on a gold adatom while tilting the PDI molecule away from the surface is shown in Figure 5C and 5D. This yields a stable structure with the PDI molecule tilted at ~35° to the Au(111) surface and is only ~30 kJ/mol less stable than the oligomer chain shown in Figure 5C and 5D. The effect of the location of the co-adsorbed CO molecule was not investigated in detail since the aim of the calculation is to explore whether the stabilization of an intermediate, decoordinated PDI state by CO adsorption was possible. This intermediate state will create additional CO adsorption sites adjacent to the $–(Au–PDI)_n–$ oligomer chain. Continuing this process will lead to the formation of an array of Au–PDI adatom complexes surrounded by CO molecules as imaged in Figure 3.

This process is observed experimentally to be reversible. Heating the surface causes CO to desorb and the infrared modes due to the initial $–(Au–PDI)_n–$ oligomer chain to reappear (Figure 1). Similar effects appear to occur also for $–(Au–PDI)_n–$ oligomers bridging gold nanoparticles on a mica substrate (Figure 4).[18] Here, the oligomer chain is proposed to form by removing gold atoms from the nanoparticles on the mica surface. This oligomer environment differs from that of the chains on A(111) since the substrate binding for CO will be weaker on mica than on gold, emphasizing the importance of the interaction between the CO $2\pi^*$ orbitals with the gold adatom. Strong overlap of the $2\pi^*$ orbitals of CO with adjacent metals atoms has been seen for CO adsorbed in the four-fold hollow site of Mo(100) where extremely large decreases in CO stretching frequency are found.[51] Figure 4 shows the variation in sheet resistance as a function of CO pressure and displays two distinct regions with a transition between them at a CO pressure of ~400 Torr. Note that these are not adsorption isotherms. Nevertheless, the two region of conductivity change are likely to correspond to the above observation of two CO adsorption sites. This would indicate that the initial conductivity change at low pressures is due to CO adsorbing adjacent to the $–(Au–PDI)_n–$ oligomer chain while the more rapid conductivity change at higher pressures

ACS Paragon Plus Environment

correlates with chain disruption to form an array of Au–PDI adatom complexes. The origin of the initial resistance change is not clear, but may be due to a modification of the electronic structure of the chain by CO co-adsorption..

Conclusions

The results clearly show reversible adsorption of carbon monoxide on –(Au–PDI)$_n$– oligomer chains on Au(111) that causes a change in chain structure to produce Au–PDI adatom complexes that stabilize CO adsorption and create additional CO adsorption sites. The combined infrared and STM results show that CO initially adsorbs adjacent to one side of the oligomer chain thereby strengthening both the Au–C≡N bond and increasing the CO adsorption energy consistent with the isocyanide acting as a σ-donor and CO as a π-acceptor. The electronic perturbation is suggested to result in a resistance increase of a PDI-linked nanoparticle array on mica. Isocyanide binding in the Au–PDI adatom complex is similarly enhanced by CO co-adsorption. This surface restructuring exposes additional CO binding sites where the chain disruption causes a further resistance increase in the nanoparticle array.

These effects are analogous to allosteric oxygen, CO and NO adsorption by hemoglobin.[2] However, in the case of the –(Au–PDI)$_n$– oligomers, the thermodynamics of the decoordination pathway are not enhanced by CO co-adsorption since CO stabilizes both the initial <u>and</u> final states.[52-53] Instead a kinetic "foot-in-the-door" model is proposed in which fluctuations in the PDI bonding to a gold adatom in the oligomer chain allows CO to diffuse from adjacent adsorption sites to prevent the back reaction from occurring. Further adsorption onto sites adjacent to the oligomer chain will prevent CO diffusion away from inter-adatom adsorption sites allowing the eventual formation of an array of Au–PDI adatom complexes surrounded by co-adsorbed CO, thereby rendering the overall process exothermic. The process is reversible; heating the surface to desorb CO restores the oligomer chains.[19]

Since this process does not rely on intermolecular interactions weakening the initial-state energy or strengthening the final state, and is purely a kinetic effect in which the reverse reaction is inhibited, it can be expected to be a general phenomenon and to occur with other adsorbates.

Acknowledgements

We thank Professor Hans-Joachim Freund for useful discussions.

Supporting Information

Supporting Information Available: Includes Figures S1 and S2. This material is available free of charge *via* the Internet at http://pubs.acs.org.

References

1. Perutz, M. F., *Mechanisms of Cooperativity and Allosteric Regulation in Proteins*; Cambridge University Press: Cambridge, U.K., 1990.
2. Petsko, G. A; . Ringe. D., *Protein Structure and Function*; Sinauer Associates: Sunderland, MA, 2004.
3. Sato, H.; Kosaka, W.; Matsuda, R.; Hori, A.; Hijikata, Y.; Belosludov, R. V.; Sakaki, S.; Takata, M.; Kitagawa, S., Self-Accelerating Co Sorption in a Soft Nanoporous Crystal. *Science* **2014**, *343*, 167-170.
4. Boscoboinik, J. A.; Calaza, F. C.; Habeeb, Z.; Bennett, D. W.; Stacchiola, D. J.; Purino, M. A.; Tysoe, W. T., One-Dimensional Supramolecular Surface Structures: 1,4-Diisocyanobenzene on Au(111) Surfaces. *Phys. Chem. Chem. Phys.* **2010**, *12*, 11624-11629.

5. Swanson, S. A.; McClain, R.; Lovejoy, K. S.; Alamdari, N. B.; Hamilton, J. S.; Scott, J. C., Self-Assembled Diisocyanide Monolayer Films on Gold and Palladium. *Langmuir* **2005**, *21*, 5034-5039.

6. Dahlke, R.; Schollwöck, U., Electronic Transport Calculations for Self-Assembled Monolayers of 1,4-Phenylene Diisocyanide on Au(111) Contacts. *Phys. Rev. B* **2004**, *69*, 085324.

7. Stapleton, J. J.; Daniel, T. A.; Uppili, S.; Cabarcos, O. M.; Naciri, J.; Shashidhar, R.; Allara, D. L., Self-Assembly, Characterization, and Chemical Stability of Isocyanide-Bound Molecular Wire Monolayers on Gold and Palladium Surfaces. *Langmuir* **2005**, *21*, 11061-11070.

8. Li, Y.; Lu, D.; Swanson, S. A.; Scott, J. C.; Galli, G., Microscopic Characterization of the Interface between Aromatic Isocyanides and Au(111): A First-Principles Investigation. *J. Phys. Chem. C.* **2008**, *112*, 6413-6421.

9. Murphy, K. L.; Tysoe, W. T.; Bennett, D. W., A Comparative Investigation of Aryl Isocyanides Chemisorbed to Palladium and Gold: An Atr-Ir Spectroscopic Study. *Langmuir* **2004**, *20*, 1732-1738.

10. Kim; Beebe, J. M.; Jun, Y.; Zhu, X. Y.; Frisbie, C. D., Correlation between Homo Alignment and Contact Resistance in Molecular Junctions: Aromatic Thiols Versus Aromatic Isocyanides. *J. Am. Chem. Soc.* **2006**, *128*, 4970-4971.

11. Zhou, J.; Acharya, D.; Camillone, N.; Sutter, P.; White, M. G., Adsorption Structures and Electronic Properties of 1,4-Phenylene Diisocyanide on the Au(111) Surface. *J. Phys. Chem. C.* **2011**, *115*, 21151-21160.

12. Robertson, M. J.; Angelici, R. J., Adsorption of Aryl and Alkyl Isocyanides on Powdered Gold. *Langmuir* **1994**, *10*, 1488-1492.

13. Shih, K.-C.; Angelici, R. J., Equilibrium and Saturation Coverage Studies of Alkyl and Aryl Isocyanides on Powdered Gold. *Langmuir* **1995**, *11*, 2539-2546.

14. Angelici, R. J.; Lazar, M., Isocyanide Ligands Adsorbed on Metal Surfaces: Applications in Catalysis, Nanochemistry, and Molecular Electronics. *Inorg. Chem.* **2008**, *47*, 9155-9165.

15. Gruenbaum, S. M.; Henney, M. H.; Kumar, S.; Zou, S., Surface-Enhanced Raman Spectroscopic Study of 1,4-Phenylene Diisocyanide Adsorbed on Gold and Platinum-Group Transition Metal Electrodes. *J. Phys. Chem. B.* **2006**, *110*, 4782-4792.

16. Bae, S. J.; Lee, C.-r.; Choi, I. S.; Hwang, C.-S.; Gong, M.-s.; Kim, K.; Joo, S.-W., Adsorption of 4-Biphenylisocyanide on Gold and Silver Nanoparticle Surfaces: Surface-Enhanced Raman Scattering Study. *J. Phys. Chem. B.* **2002**, *106*, 7076-7080.

17. Feng, M.; Sun, H.; Zhao, J.; Petek, H., Self-Catalyzed Carbon Dioxide Adsorption by Metal–Organic Chains on Gold Surfaces. *ACS Nano* **2014**, *8,* 8644-8652

18. Kestell, J.; Abuflaha, R.; Boscoboinik, J. A.; Bai, Y.; Bennett, D. W.; Tysoe, W. T., Linking Gold Nanoparticles with Conductive 1,4-Phenylene Diisocyanide-Gold Oligomers. *Chem. Commun.* **2013**, *49*, 1422-1424.

19. Garvey, M.; Kestell, J.; Abuflaha, R.; Bennett, D. W.; Henkelman, G.; Tysoe, W. T., Understanding and Controlling the 1,4-Phenylene Diisocyanide–Gold Oligomer Formation Pathways. *J. Phys. Chem. C.* **2014**, *118*, 20899-20907.

20. Efraty, A.; Feinstein, I.; Frolow, F.; Wackerle, L., Two-Dimensional Coordination Polymers of Rhodium(1+) with Rigid Collinear Diisocyanide Bridges and Stacked Layers Arrangement. *J. Am. Chem. Soc.* **1980**, *102*, 6341-6343.

21. Feinstein-Jaffe, I.; Efraty, A., Electrical Semiconductivity of Stacked Layer Coordination Polymers of Rhodium(I). *Macromolecules* **1986**, *19*, 2076-2077.

22. Carson, C. G.; Gerhardt, R. A.; Tannenbaum, R., Chemical Stability and Characterization of Rhodium-Diisocyanide Coordination Polymers. *J. Phys. Chem. B.* **2007**, *111*, 14114-14120.

23. Lawrence, S. A.; Sermon, P. A.; Feinstein-Jaffe, I., An Investigation into the Role of Cooperative Effects in Polymeric Rhodium(I) Bis-4,4'-Diisocyanobiphenyl Chloride Catalysts in Olefin Hydrogenation Reactions. *J. Mol. Catal.* **1989**, *51*, 117-127.

24. Kestell, J.; Abuflaha, R.; Boscoboinik, J. A.; Garvey, M.; Bennett, D. W.; Tysoe, W. T., Determination of Adsorbate Structures from 1,4-Phenylene Diisocyanide on Gold. *J. Phys. Chem. Lett.* **2014**, *5*, 3577-3581.

25. Kaltchev, M.; Thompson, A. W.; Tysoe, W. T., Reflection-Absorption Infrared Spectroscopy of Ethylene on Palladium (111) at High Pressure. *Surf. Sci.* **1997**, *391*, 145-149.

26. Kresse, G.; Joubert, D., From Ultrasoft Pseudopotentials to the Projector Augmented-Wave Method. *Phys. Rev. B.* **1999**, *59*, 1758-1775.

27. Blöchl, P. E., Projector Augmented-Wave Method. *Phys. Rev. B.* **1994**, *50*, 17953-17979.

28. Kresse, G.; Hafner, J., Ab Initio Molecular Dynamics for Liquid Metals. *Phys. Rev. B.* **1993**, *47*, 558-561.

29. Kresse, G.; Furthmüller, J., Efficient Iterative Schemes for Ab Initio Total-Energy Calculations Using a Plane-Wave Basis Set. *Phys. Rev. B.* **1996**, *54*, 11169-11186.

30. Kresse, G.; Furthmüller, J., Efficiency of Ab-Initio Total Energy Calculations for Metals and Semiconductors Using a Plane-Wave Basis Set. *Comput. Mater. Sci.* **1996**, *6*, 15-50.

31. Perdew, J. P.; Burke, K.; Ernzerhof, M., Generalized Gradient Approximation Made Simple. *Phys. Rev. Lett.* **1996**, *77*, 3865-3868.

32. Tkatchenko, A.; Scheffler, M., Accurate Molecular Van Der Waals Interactions from Ground-State Electron Density and Free-Atom Reference Data. *Phys. Rev. Lett.* **2009**, *102*, 073005.

33. Boscoboinik, J.; Kestell, J.; Garvey, M.; Weinert, M.; Tysoe, W., Creation of Low-Coordination Gold Sites on Au(111) Surface by 1,4-Phenylene Diisocyanide Adsorption. *Top. Catal.* **2011**, *54*, 20-25.

34. Ruggiero, C.; Hollins, P., Adsorption of Carbon Monoxide on the Gold(332) Surface. *J. Chem. Soc., Faraday Trans.* **1996**, *92*, 4829-4834.

35. Bradshaw, A. M.; Pritchard, J., Infrared Spectra of Carbon Monoxide Chemisorbed on Metal Films: A Comparative Study of Copper, Silver, Gold, Iron, Cobalt and Nickel. *Proc. R. Soc. London, Ser. A* **1970**, *316*, 169-183.

36. Kottke, M. L.; Greenler, R. G.; Tompkins, H. G., An Infrared Spectroscopic Study of Carbon Monoxide Adsorbed on Polycrystalline Gold Using the Reflection-Absorption Technique. *Surf. Sci.* **1972**, *32*, 231-243.

37. Meier, D. C.; Goodman, D. W., The Influence of Metal Cluster Size on Adsorption Energies: Co Adsorbed on Au Clusters Supported on TiO_2. *J. Am. Chem. Soc.* **2004**, *126*, 1892-1899.

38. Hrbek, J.; Hoffmann, F. M.; Park, J. B.; Liu, P.; Stacchiola, D.; Hoo, Y. S.; Ma, S.; Nambu, A.; Rodriguez, J. A.; White, M. G., Adsorbate-Driven Morphological Changes of a Gold Surface at Low Temperatures. *J. Am. Chem. Soc.* **2008**, *130*, 17272-17273.

39. Piccolo, L.; Loffreda, D.; Aires, F.; Deranlot, C.; Jugnet, Y.; Sautet, P.; Bertolini, J. C., The Adsorption of Co on Au(111) at Elevated Pressures Studied by Stm, Rairs and Dft Calculations. *Surf. Sci.* **2004**, *566*, 995-1000.

40. Henderson, J. I.; Feng, S.; Bein, T.; Kubiak, C. P., Adsorption of Diisocyanides on Gold. *Langmuir* **2000**, *16*, 6183-6187.

41. Ito, M.; Noguchi, H.; Ikeda, K.; Uosaki, K., Substrate Dependent Structure of Adsorbed Aryl Isocyanides Studied by Sum Frequency Generation (Sfg) Spectroscopy. *Phys. Chem. Chem. Phys.* **2010**, *12*, 3156-3163.

42. Boscoboinik, J.; Kestell, J.; Garvey, M.; Weinert, M.; Tysoe, W. T., Creation of Low-Coordination Gold Sites on Au(111) Surface by 1,4-Phenlyene Diisocyanide Adsorption. *Top. Catal* **2011**, *54,* 20-25

43. Clark, A., *The Theory of Adsorption and Catalysis*; Academic Press: New York, 1970.

44. Hammer, B.; Morikawa, Y.; Nørskov, J. K., Co Chemisorption at Metal Surfaces and Overlayers. *Phys. Rev. Lett.* **1996**, *76*, 2141-2144.

45. Redhead, P. A., Thermal Desorption of Gases. *Vacuum* **1962**, *12*, 203-211.

46. Liao, K.; Fiorin, V.; Gunn, D. S. D.; Jenkins, S. J.; King, D. A., Single-Crystal Adsorption Calorimetry and Density Functional Theory of Co Chemisorption on Fcc Co{110}. *Phys. Chem. Chem. Phys.* **2013**, *15*, 4059-4065.

47. Gilman, Y.; Allen, P. B.; Hybertsen, M. S., Density-Functional Study of Adsorption of Isocyanides on a Gold (111) Surface. *J. Phys. Chem. C.* **2008**, *112*, 3314-3320.

48. Newns, D. M., Self-Consistent Model of Hydrogen Chemisorption. *Phys. Rev.* **1969**, *178*, 1123-1135.

49. Li, Y.; Lu, D. Y.; Swanson, S. A.; Scott, J. C.; Galli, G., Microscopic Characterization of the Interface between Aromatic Isocyanides and Au(111): A First-Principles Investigation. *J. Phys. Chem. C* **2008**, *112*, 6413-6421.

50. Blyholder, G., Molecular Orbital View of Chemisorbed Carbon Monoxide. *The J. Phys. Chem.* **1964**, *68*, 2772-2777.

51. Zaera, F.; Kollin, E.; Gland, J. L., Observation of an Unusually Low C-O Stretching Frequency: Co Chemisorption on a Mo(100) Surface. *Chem. Phys. Lett.* **1985**, *121*, 464-468.

52. Monod, J.; Wyman, J.; Changeux, J.-P., On the Nature of Allosteric Transitions: A Plausible Model. *J. Mol. Biol.* **1965**, *12*, 88-118.

53. Koshland, D. E.; Némethy, G.; Filmer, D., Comparison of Experimental Binding Data and Theoretical Models in Proteins Containing Subunits. *Biochemistry* **1966**, *5*, 365-385.

Figure Captions

Figure 1: A: A series of RAIRS spectra of CO adsorbed on a PDI-saturated Au(111) surface. The bottom spectrum is for PDI adsorbed on the Au(111) surface at 300 K. The sequence of spectra shows the effect of CO dosing (CO Dose (100K)/10^{-4} Torr s) at 100 K. The CO doses (in units of 10^{-4} Torr s) are indicated above the corresponding spectrum. The top five spectra show the effect of heating the sample to various temperature (indicated by "Heat"), where the annealing temperature are shown above the corresponding spectra. B: Infrared spectra of 3×10^{-3} Torr s of ^{12}CO (Bottom spectrum) and ^{13}CO (Top spectrum) exposed at 100 K to a Au(111) surface saturated with PDI. The lines indicate the predicted shifts in vibrational frequencies due to the effect of a change in the reduced mass of ^{13}CO.

Figure 2: Top Image: 60 nm× 60 nm scan area STM image of a PDI-saturated Au(111) surface heated to 373 K prior to CO exposure (V_b=-1.0 V, I_t =353 pA). Bottom Image: A: 40 nm× 40 nm scan area STM image of a PDI-saturated Au(111) surface exposed to 0.6 L of CO at 120 K (V_b=-1.4 V, I_t =233 pA). B: A higher resolution image of the same surface indicating the location of the co-adsorbed CO.

Figure 3: A: 30 nm× 30 nm scan area STM image of a PDI-saturated Au(111) surface exposed to 3.6 L of CO at 120 K (V_b=-1.37 V, I_t =367 pA). B: A higher resolution image of the same surface with line profile C: between and D: along the chains.

Figure 4: A: Percent enhancement in resistance when pressurizing gold nanoparticles (average diameter ~ 8 nm) saturated with PDI in vacuo with low pressures (up to 5 Torr total) of CO at a sample temperature of 290 K, while raising (■) and lowering (□) the pressure and B: The same experiment carried out up to a CO pressure of 760 Torr. Shown as an inset is the variation in resistance as a function of CO pfressures collected without dosing the nanoparticle array with PDI.

Figure 5: A: Top and B: Side views of the most stable –(Au–PDI)$_n$– oligomer chain on a Au(111) surface showing two repeat units calculated using an 8×4 unit cell, C: Top and D: Side views of the most stable structure formed by decoordinating one end of a PDI molecule linking between gold adatoms and adsorbing a CO molecule to the gold adatom demonstrating that this forms a stable structure.

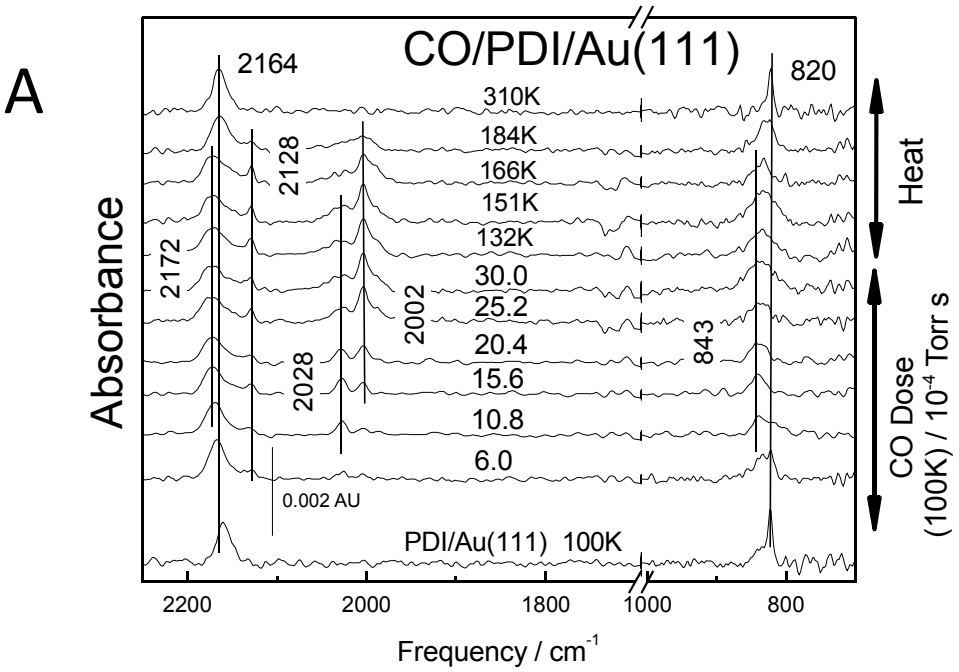

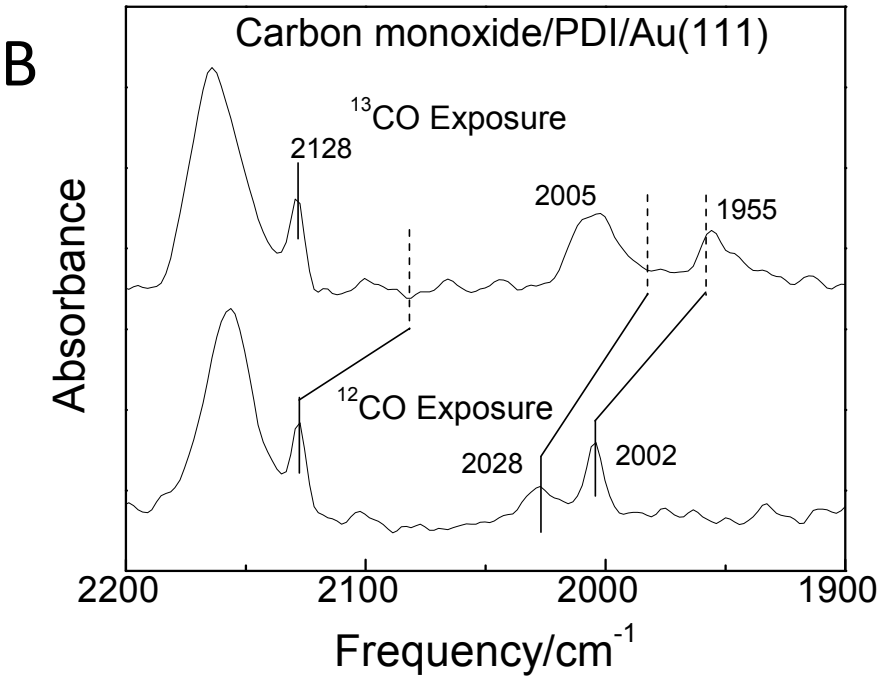

Kestell *et al*, Figure 1

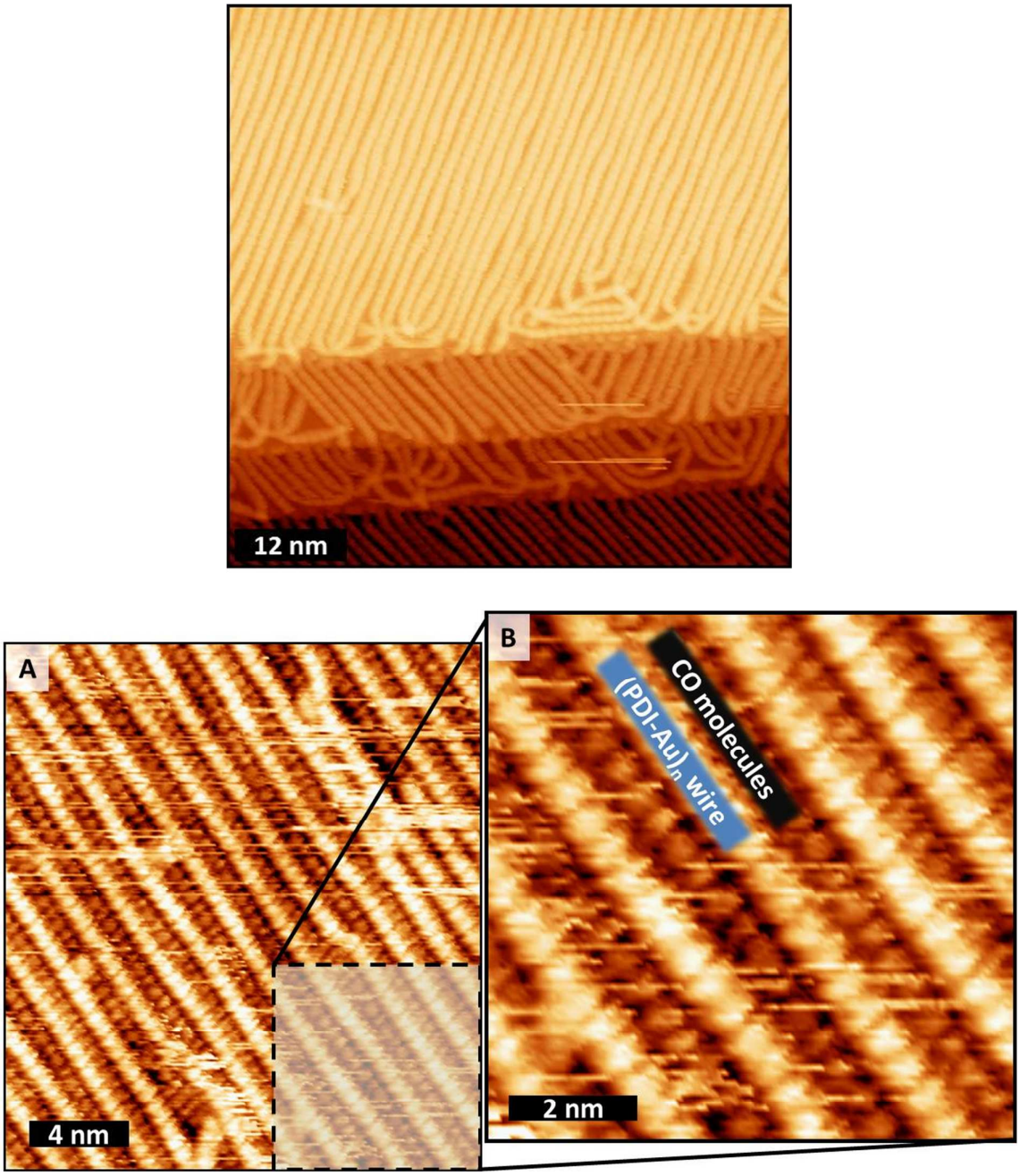

Kestell *et al*, Figure 2

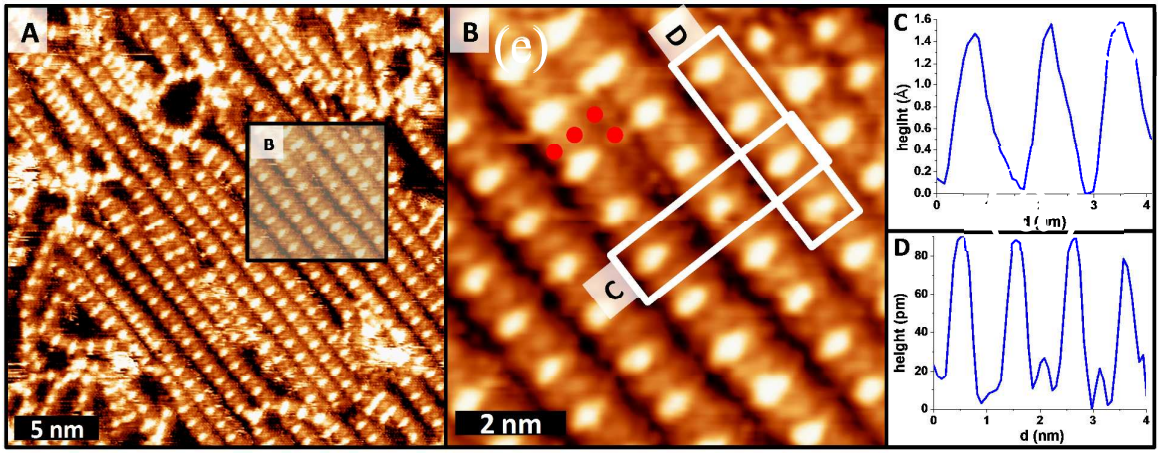

Kestell *et al*, Figure 3

A

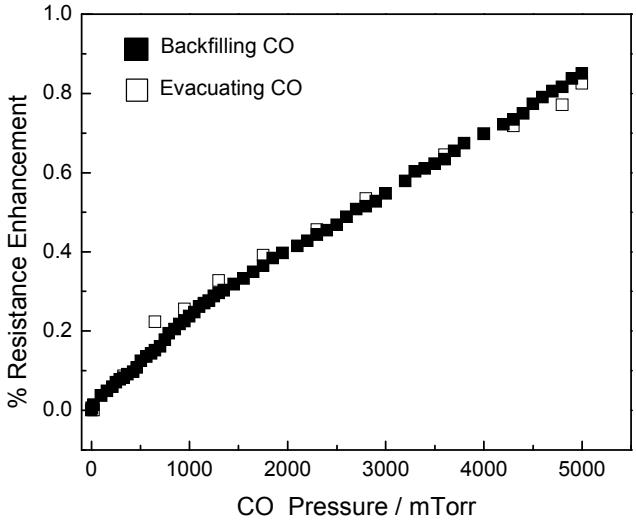

B

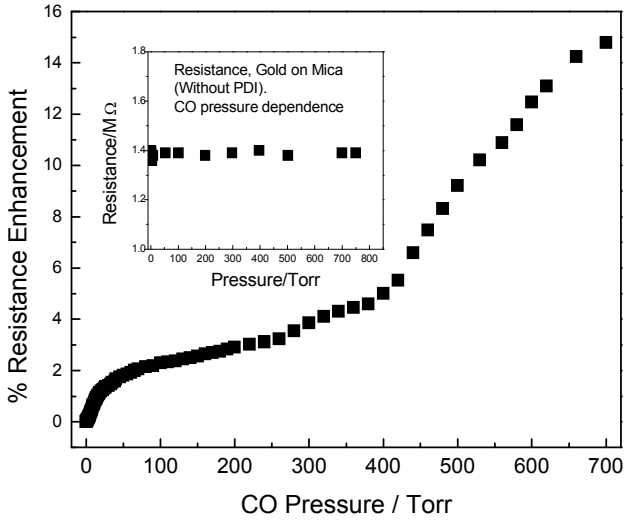

Kestell *et al*, Figure 4

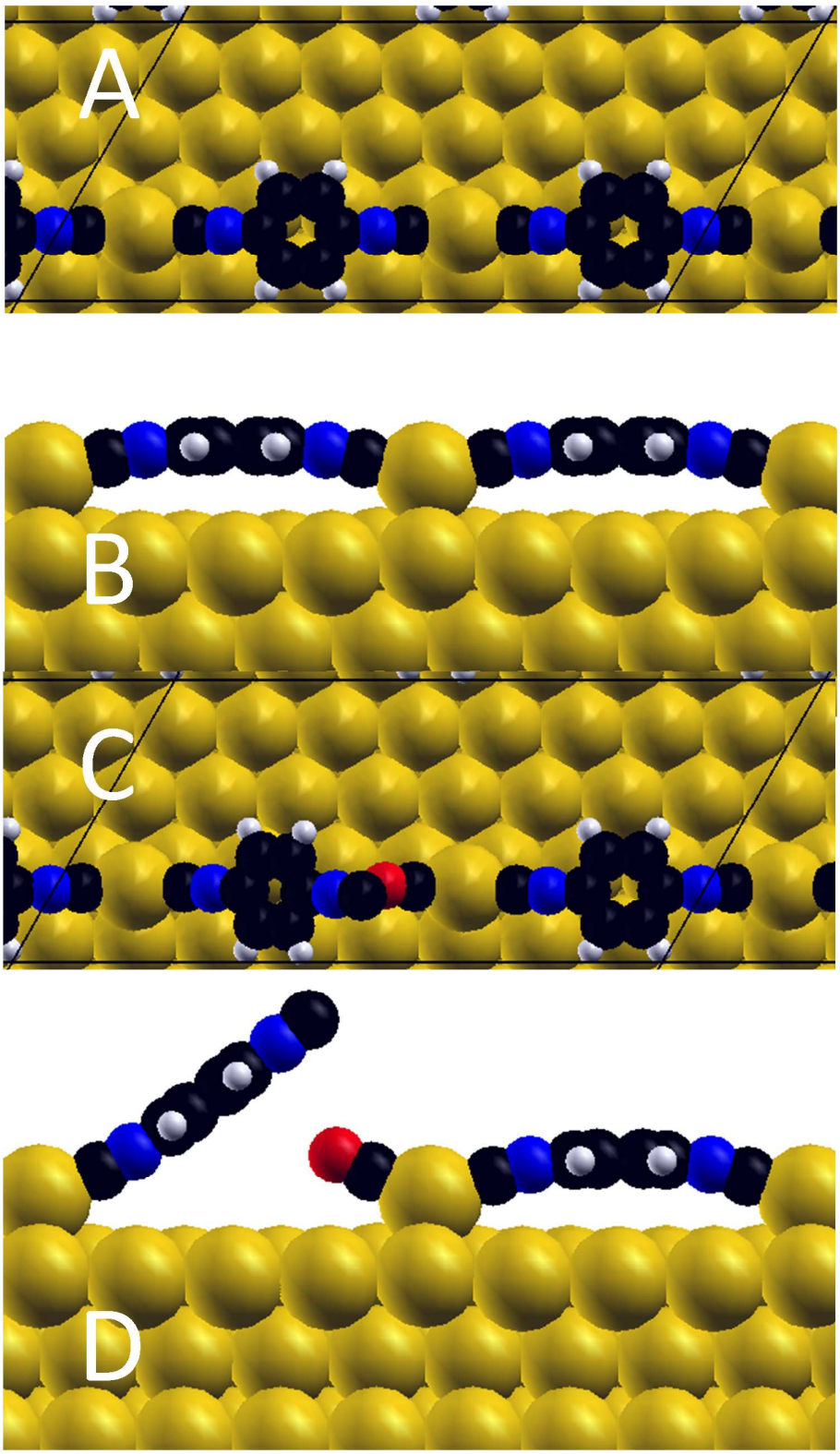

Kestell *et al*, Figure 5

Tables

Table 1: CO adsorption energy and energy stabilization of PDI in a –(Au–PDI)$_n$– oligomer chain following CO adsorption at various sites adjacent to the –(Au–PDI)$_n$– oligomer chain, where the adsorption sites are shown in Figure S1. Energies for sites where the CO moved to the A1 or A2 sites are not shown.

CO Adsorption Site	E_{ads}(CO) [kJ/mol]	PDI Energy Stabilization [kJ/mol]
A1	-49	-39
A2	-49	-38
A3	-	-57
	-	
B1	-	-53
B2	-	-56
B3	-	-55
	-	
H1	-	-56
H2	-	-55

Table 2: Adsorption energies of PDI on the Au–PDI adatom complex alone, and the effect of CO co-adsorption on the CO binding energy and the energy of the Au–PDI adatom complex. The adsorption sites are shown in Figure S2.

CO Adsorption Site	E_{ads} (PDI) [kJ/mol]	E_{ads} (CO) [kJ/mol]
-	152	-
A1	196	57
A2	196	53
A3	195	53
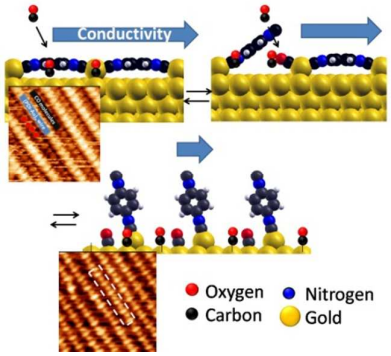
Graphical Abstract